

# Nuclear Pleomorphism Scoring by Selective Cell Nuclei Detection

Jean-Romain Dalle   Hao Li   Chao-Hui Huang   Wee Kheng Leow  
Dept. of Computer Science, National University of Singapore  
{jeanroma, liaho, huangch, leowwk}@comp.nus.edu.sg

Daniel Racoceanu  
CNRS, IPAL UMI Singapore  
danielr@comp.nus.edu.sg

Thomas C. Putti  
Dept. of Pathology, National University Hospital  
pattcp@nus.edu.sg

## Abstract

*Scoring the nuclear pleomorphism in histopathological images is a standard clinical practice for the diagnosis and prognosis of breast cancer. It relies highly on the experience of the pathologists. In a large hospital, one pathologist may have to evaluate more than a hundred cases per day, which is a very tedious and time-consuming task. Thus, it is necessary to develop an automatic system to support the pathologists. This paper proposes a method that automatically selects and segments critical cell nuclei within a high-resolution histopathological image for nuclear pleomorphism scoring according to the Nottingham grading system. In contrast, most of the existing methods tend to detect all the cells in an image which is computationally expensive. Comprehensive experiments show that accurate scoring can be achieved by segmenting only critical cells, thus reducing the execution time of the method.*

## 1. Introduction

Grading of histopathological images of breast biopsy specimens is a standard clinical practice for the diagnosis and prognosis of breast cancer development. Pathologists analyze the tissue specimens manually under a microscope. In a large hospital, they may have to analyze more than a hundred cases per day, which is a very tedious and time-consuming task. Moreover, the experience of the pathologists directly influence the accuracy of grading [8]. Thus, it is necessary to develop an automatic system to support the pathologists by providing second opinions. In addition, the system can reduce their workload, and alert them to cases that require closer attention. Consequently, the pathologists can focus more attention on the diagnosis and the prognosis of the patients.

In this paper, a new approach for fully automatic nuclear pleomorphism scoring is proposed. It selections and seg-

ments a small number of critical cell nuclei in an image for nuclear pleomorphism scoring according to the Nottingham grading system.

## 2. Related Work

Breast cancer grading is performed according to the Nottingham grading system. One important criterion of the Nottingham grading system is the score of the nuclear pleomorphism which is performed on segmented cell nuclei. Thus, many methods have been proposed for the segmentation of cell nuclei in histological images [1, 4, 6, 7, 9, 10, 2, 11, 12, 13, 14]. These methods are based on traditional algorithms like thresholding, watershed, morphological operations etc. The performance of these methods relies on the accurate segmentation of cell nuclei.

Among the existing methods, the method of Cosetto et al [4] is most relevant to our work. Their method segments cell nuclei based on the Active Contour Model (ACM) and classify them according to Support Vector machine (SVM). It is accurate but computationally expensive.

Most of the existing methods tend to detect all of the cells in the input image. In contrast, our experimental results indicate that it is not necessary to segment all the cell nuclei. Only critical cell nuclei that affect the score need to be segmented for nuclear pleomorphism scoring.

## 3. Scoring by Selective Segmentation

Our proposed method is based on the idea that the input image contains so many cell nuclei, and thus so much redundant information, that accurate nuclear pleomorphism scoring can be achieved by segmenting only the critical cell nuclei. We observed that when a pathologist evaluates a biopsy specimen under a microscope, he first browses the whole specimen to obtain a general assessment of the specimen. Next, he chooses a region of interest (ROI) that are critical to the assessment and examines the critical cell nu-

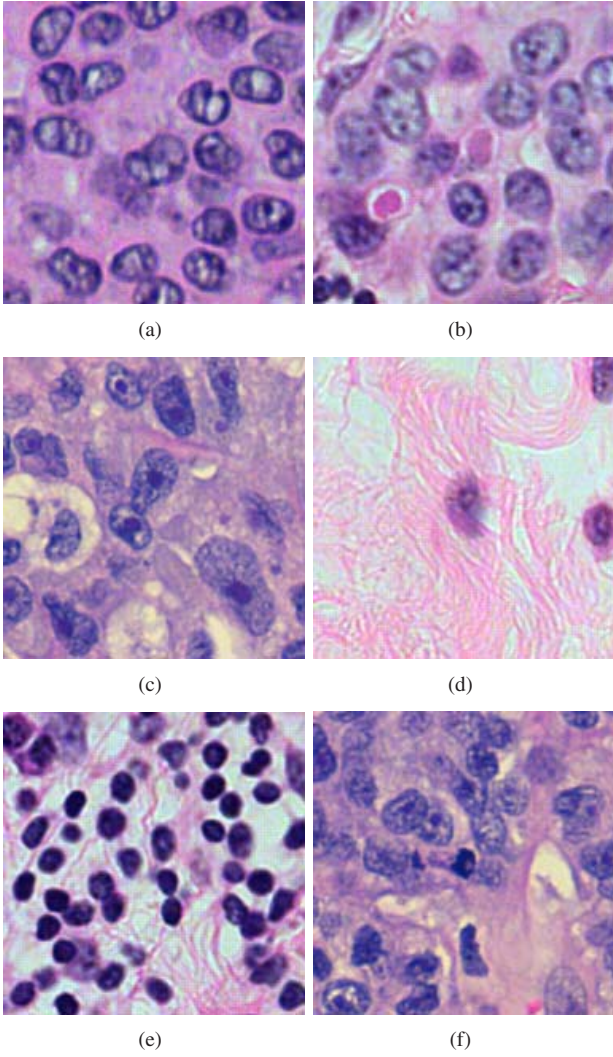


Figure 1. Various types of Cells in biopsy microimage. (a, b, c) Cancerous epithelial cells in various environment. (d) Fibroblasts. (e) Inflammatory cells. (f) Mitotic cell.

clei in these regions to score the specimen. Our method works in a similar way. Given an image of a biopsy specimen, ROI's are first detected. A method for detecting neoplasm ROI is reported in [5] and is thus omitted in this paper.

Given the ROI, candidate cell nuclei that influence nuclear pleomorphism scoring are detected (Section 3.1). These are large epithelial cell nuclei that cluster together (Fig. 1). Next, the boundaries of the candidate cell nuclei are segmented (Section 3.2) and nuclear pleomorphism score is computed based on the segmented cell nuclei (Section 3.3).

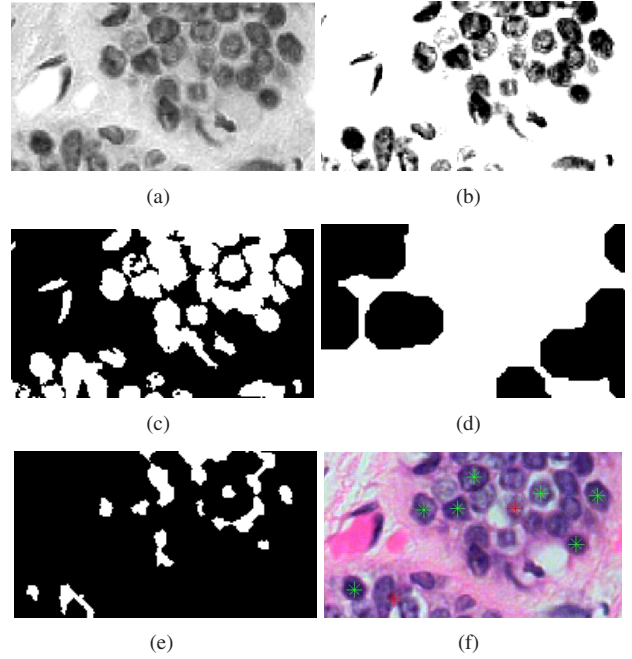


Figure 2. Candidate cell nuclei detection. (a) A region in image frame. (b) Gamma corrected image. (c) Thresholded image. (d) Detected candidates are denoted by the green crosses +.

### 3.1. Detection of Candidates

**Step 1:** The red channel  $I(x, y)$  of an input color image is extracted and enhanced by gamma correction (Fig 2(b)):

$$J(x, y) = G_{\alpha\beta}(I(x, y)), \quad (1)$$

where  $G_{\alpha\beta}$  is the gamma correction function and  $[\alpha, \beta]$  the range of values on which to apply the gamma correction.

**Step 2:** The enhanced image  $J(x, y)$  is thresholded into a binary image  $B(x, y)$  according to threshold  $T_B$  (Fig 2(c)):

$$B(x, y) = \begin{cases} 1, & \text{if } J(x, y) < T_B \\ 0, & \text{otherwise} \end{cases} \quad (2)$$

As shown in Fig 1, the critical cell nuclei, i.e., the epithelial cells, are large compared to inflammatory cells and mitotic cells. Moreover, they cluster near each other in contrast to fibroblasts. So, the algorithm aims to detect large cell nuclei that cluster near each other. This is achieved in the following steps.

**Step 3:** Morphological operator is applied to the binary image  $B(x, y)$  to dilate it. In this way, cell nuclei that cluster near each other are merged into large connected regions, whereas isolated cell nuclei remain isolated (Fig 2(d)).

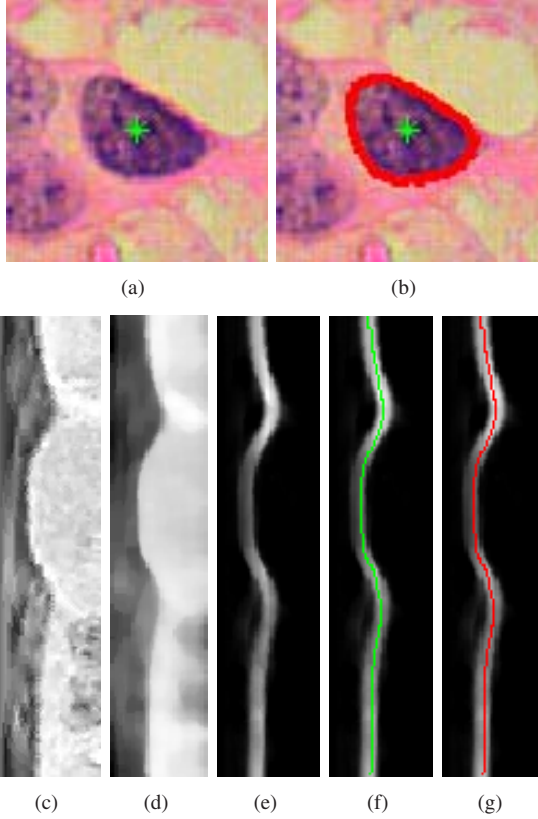


Figure 3. Steps for the Polar Transform Segmentation. (a) A patch of image containing a candidate cell nucleus and (b) its Segmented boundaries, (c) Input Image in polar space, (d) median filtering result, (e) Gradient image using Biquad, (f) first boundary detection in clockwise direction, (g) second boundary detection in anticlockwise direction .

**Step 4:** Morphological operator is applied to the dilated image  $B'(x, y)$  to erode it. In this way, epithelial cell nuclei that touch each other are disconnected into individual blobs (Fig 2(e)).

**Step 5:** Distance Transform  $D(x, y)$  is applied on the eroded image  $E(x, y)$  to compute estimated size of the individual blobs. Next, the bobs that are large enough (i.e.,  $D(x, y) > T_D$ ) and not isolated (i.e., fall in large connected regions detected in Step 3) are identified.

Next, square patches of image each containing a candidate cell nucleus are cropped and the centroids  $(x, y)$  of the cell nuclei are computed. Finally, the selected candidates are sorted in decreasing order of  $D(x, y)$  (Fig 3(a)).

### 3.2. Segmentation of Nucleus Boundaries

The segmentation of the boundaries of selected cell nuclei is processed in the polar space (Fig 3), which uses the

detected centers of cell nuclei as the origin. It consists of several steps. First, the square patches of image of  $P(x, y)$  is transformed from the Cartesian space to polar space resulting in a polar image  $P(\theta, r)$ :

$$x = r \cos \theta \text{ and } y = r \sin \theta, \quad (3)$$

where  $r$  denotes the radius, and  $\theta$  the angle. Next, a median filtering is performed on the patch  $P(\theta, r)$  to reduce the noise and preserve edges. Then, the gradient  $G(\theta, r)$  of the filtered image is computed using Biquad filtering.

Next, the segmentation algorithm processes each patch of gradient image  $G(\theta, r)$  in two steps: initialization and iteration. *Initialization:* For each angle  $\theta_0$  of the gradient image  $G(\theta_0, r)$ , the pixel with highest value along the radius dimension is identified.

Then, the identified pixels close to each other within a distance  $d$  are connected into segments. The longest segment is considered as part of the correct boundary and therefore the pixel  $(\theta_0, r_0)$  located at the middle of this segment is used as reference point for the iterative part.

*Iteration:* The iteration starts using the reference point  $(\theta_0, r_0)$  to compute parameters (Eq. 4) using the Gradient image  $G(\theta, r)$  and the Input Image  $I(\theta, r)$  at an angle  $\theta_1$ :

$$\begin{cases} \delta_G(\theta_1, r) &= G(\theta_1, r) - G(\theta_0, r_0) \\ \delta_I(\theta_1, r) &= I(\theta_1, r) - I(\theta_0, r_0) \end{cases} \quad (4)$$

These parameters are combined linearly in a cost function  $C(\theta_1, r)$  (Eq. 5):

$$C(\theta_1, r) = G_{\mu, \sigma}^2 (\alpha \delta_G(\theta_1, r) + \beta \delta_I(\theta_1, r)), \quad (5)$$

where  $G_{\mu, \sigma}$  is a gaussian weight along the radius with a mean  $\mu = r_0$  and  $\sigma = 3$ ,  $\alpha$  and  $\beta$  are weights.

The pixel with the highest value is then identified as the new reference point  $(\theta_0, r_0)$  and the angle  $\theta_0$  is incremented, and this step iterates until the end of the image is reached. After identifying the reference point  $\theta_i, r_i$ , a low-order polynomial curve is fitted to the reference points to obtain the segmented boundary.

The iterative part is processed twice, in clockwise and anticlockwise directions, for increased noise resilience. Among the two boundaries produced, the one with the highest energy is selected as the correct boundary.

### 3.3. Nuclear Pleomorphism Scoring

According to the Nottingham grading system [3], pathologists score nuclear pleomorphism as follow:

- Score 1: Nuclei small with little increase in size in comparison with normal breast epithelial cells, regular outlines, uniform nuclear chromatin, little variation in size.

- Score 2: Cells larger than normal with open vesicular nuclei, visible nucleoli and moderate variability in both size and shape

- Score 3: Vesicular nuclei, often with prominent nucleoli, exhibiting marked variation in size and shape, occasionally with very large and bizarre form

Thus, we applied a scoring based on the size, shape and texture of the segmented epithelial cell nuclei. The size criteria combines the mean and standard deviation of the population of the segmented cell nuclei. The shape is computed using the roundness criteria for each cell nuclei segmented:

$$R = \frac{1}{P}4\pi A^2, \quad (6)$$

where  $A$  is the area of the object, and  $P$  is the perimeter of the object. Finally, texture is computed as the mean of the grayscale value for each individual segmented cell nuclei.

These features are used as parameters to build a Gaussian Model (Eq. 7)

$$g(u; \mu, \Sigma) = \frac{1}{\sqrt{(2\pi)^m |\Sigma|}} \exp \left[ -\frac{1}{2} (u - \mu)^T \Sigma^{-1} (u - \mu) \right] \quad (7)$$

where  $u$  is the testing data vector,  $\Sigma$  the covariance matrix and  $\mu$  the mean data computed during the training.

## 4. Experiments and Discussion

Two main experiments were performed to evaluate the accuracy of cell nuclei segmentation and nuclear pleomorphism scoring. The images are digital frames stained with H&E and magnified at 40x resolution with a scale of  $0.09\mu m^2$  / pixel, and were processed using a Quad Core 2.3 GHz and Matlab R2008a.

### 4.1. Cell Nuclei Segmentation

To measure the accuracy of cell nuclei segmentation, we compared the segmentation done by the algorithm with manual segmentation. For this test, 4 patients were used: 2 patients NP-scored 2 and 2 patients NP-scored 3. For each patient, 5 image frames were randomly selected. For each image frame, cell nuclei were manually segmented. This analysis totals 840 cell nuclei manually segmented which were compared to the same 840 cell nuclei segmented by the algorithm. An estimated segmentation accuracy error was computed using:

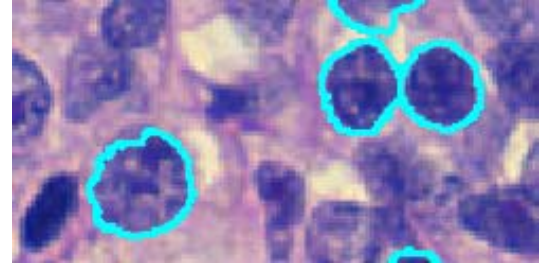
$$E = 2 \frac{C_a \cap C_m}{C_a \cup C_m} \quad (8)$$

where  $E$  is the percentage of accuracy error,  $C_a$  is the cell nuclei object segmented by the algorithm and  $C_m$  is the cell nuclei object segmented manually.

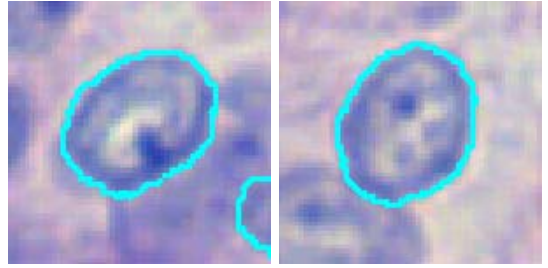
The overall accuracy error is 15.9% and there is a slight difference in accuracy error between image frames scored



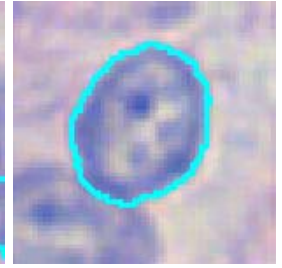
(a)



(b)



(c)



(d)



(e)



(f)

Figure 4. Results of cell nuclei segmentation.

2 and image frames scored 3 with a respective accuracy error of 15.3% and 16.5%. The accuracy error is mainly explained by the fact that the technician segmented manually the inner boundary of the cell nuclei while the algorithm detected the outer boundary. The thickness between the inner and the outer is due to the staining chemical.

### 4.2. Nuclear Pleomorphism Scoring

The test set is composed by 6 patients biopsy micro-images: 1 patient had NP score 2, and 5 had NP score 3,

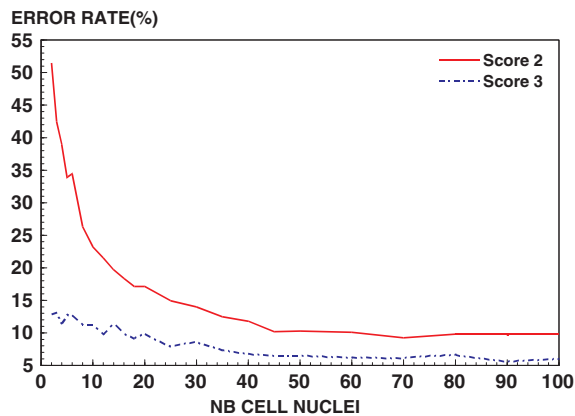


Figure 5. Error Rate of Nuclear Pleomorphism Scoring according to number of cell nuclei segmented.

as scored by the pathologist. This test set is organized as follows:

- Score-2 set: 1156 image frames located in ROI of 1 patient's image.
- Score-3 set: 1240 image frames located in ROI of 5 patients' images.

Altogether, the database used for scoring nuclear pleomorphism regroups 2396 images frames.

We assumed that within a region of interest, the score for each image frame is equal to the global score given by the pathologist. Hence, the performance of the algorithm in scoring nuclear pleomorphism was measured by comparing the scoring assessed by the classifier for each image frame with the score given by the pathologist. This gives the accuracy error of the classification.

The procedure was done as following:

- 10% of the frames for each scoring group were randomly selected to trained the classifier by modeling Gaussian for each score.
- The remaining 90% of the frames were processed and classified for the testing part.

As results, the overall accuracy of the classifier was measured (Section 4.2.1). In addition, the error accuracy for both scoring group was computed while varying the number of cell nuclei segmented within the image frame (Section 4.2.2). Finally, computational time was measured according to the number of cell nuclei segmented (Section 4.2.3) to comfort the idea that segmenting cell nuclei is expensive in computational time and segmenting limited number of critical cell nuclei is essential.

#### 4.2.1 Overall Accuracy

This analysis regroups both scoring group. In addition, the algorithm segmented as many cell nuclei as possible. Therefore, this result provides the general accuracy of the

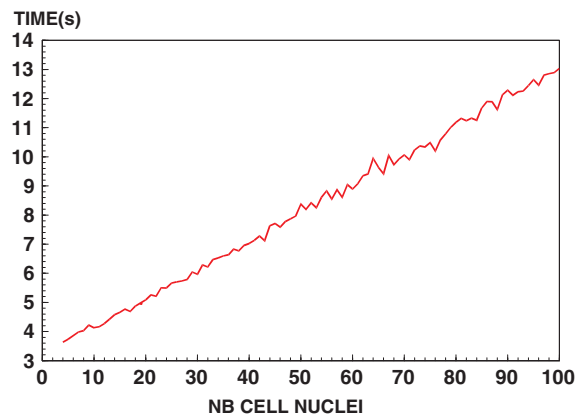


Figure 6. Computational time according to number of segmented cell nuclei.

classifier without any constraint. The overall accuracy error of the classification is 7.84%.

#### 4.2.2 Accuracy vs Number of Segmented Cell Nuclei

We applied the algorithm on both scoring group while varying the number of cell nuclei to segment. The classifier scored the different sized population of cell nuclei and we measured the accuracy error (Fig. 5). The result shows the stability of the classifier for a minimal number of cell nuclei segmented. In addition, it shows that the accuracy error converges to a minimal error for both scoring group:

- A minimum error rate of 7.8% starting from 40 cell nuclei nuclei for score 3 database.
- A minimum error rate of 12% starting from 50 cell nuclei for score 2 database.

Therefore, it shows that scoring nuclear pleomorphism over a population can be done with a limited number of critical cell nuclei.

#### 4.2.3 Computational Time

Computational time was measured for various number of cell nuclei segmented. As expected, the computational time is proportional to the number of cell nuclei segmented (Fig. 6). Therefore, segmentation of cell nuclei is a computationally expensive process.

As we noticed in the previous section 4.2.2, scoring nuclear pleomorphism can be reached with a good accuracy with a limited number of cell nuclei segmented. Hence, segmenting only a limited number of critical cell nuclei is a good way to score nuclear pleomorphism while saving computational time.

## 5. Conclusion

An automatic nuclear pleomorphism scoring method based on critical cell selection is proposed. Different to the existing algorithms, the proposed approach does not segment all of the cell nuclei in a frame. It selects only critical cell nuclei and assesses a score according to the population of cell nuclei detected. It avoids expensive computational time and provides a good accuracy in the classification.

## 6. Acknowledgement

This research is supported by A\*STAR SERC 0521010103 (NUS R-252-000-319-305).

## References

- [1] M. E. Adawi, Z. Shehab, H. Keshk, and M. E. Shourbagy. A fast algorithm for segmentation of microscopic cell images. In *Proc. of 4th Int. conf. on Information and Communications Technology*, 2006.
- [2] Y. Al-Kofahi and B. R. W. Louassed and, W. Lee and. Improved automatic detection and segmentation of cell nuclei in histopathology images. In *IEEE Trans Biomed Eng 2009*, 2009.
- [3] G. Bussolati, C. Marchio, L. Gaetano, R. Lupo, and A. Sapino. Pleomorphism of the nuclear envelope in breast cancer: a new approach to an old problem. *Journal of Cellular and Molecular Medicine*, 12:209–218, 2008.
- [4] E. Cosatto, M. Miller, H. P. Graf, and J. S. Meyer. Grading nuclear pleomorphism in histopathological micrographs. In *International Conference on Pattern Recognition*, 2008.
- [5] J. R. Dalle, W. K. Leow, D. Racoceanu, A. Tutac, and T. Putti. Automated breast cancer grading for histopathological images. In *Proc. of 30th Int. conf. of the IEEE Eng. in Medicine and Biology Society*, pages 3052–3055, 2008.
- [6] C. Demir and B. Yener. Automated cancer diagnosis based on histopathological images: a systematic survey. Technical report, Rensselaer Polytechnic Institute, 2005.
- [7] S. Doyle, M. Hwang, M. Feldman, and J. Tomaszewski. Automated grading of prostate cancer using architectural and textural image features. In *Proc. of 4th IEEE Int. Symp. on Biomedical Imaging*, pages 1284–1287, 2007.
- [8] B. Dunne and J. J. Going. Scoring nuclear pleomorphism in breast cancer. In *Histopathology*, volume 39, pages 259–265, 2001.
- [9] A. S. Jadhav, P. Banarjee, K. Chaudhuri, and J. Chatterjee. Quantitative analysis of histopathological features of precancerous lesion and condition using image processing techniques. In *Proc. of 19th IEEE Int. Symp. on Computer-Based Medical Systems*, pages 231–236, 2006.
- [10] H. Jeong, T.-Y. Kim, H.-G. Hwang, and H.-J. Choi. Comparison of thresholding methods for breast tumor cell segmentation. In *Proc. of 7th Int. Workshop on Enterprise networking and Computing in Healthcare Industry*, pages 392–395, 2005.
- [11] A. Nedzved, S. Ablameyko, and I. Pitas. Morphological segmentation of histology cell images. In *Proc. Int. Conf. Pattern Recognition*, pages 1500–1503, 2000.
- [12] F. Schnorrenberg. Comparison of manual and computer-aided breast cancer biopsy grading. In *Proc. of IEEE EMBS*, 1996.
- [13] H. Soltanian-Zadeh and K. Jafari-Khouzani. Multi-wavelet grading of prostate pathological images. In *IEEE Trans. on Biomedical Engineering*, volume 50, pages 697–704, 2003.
- [14] A. Tutac, D. Racoceanu, T. Putti, W. Xong, W.-K. Leow, and V. Cretu. Knowledge-guided semantic indexing of breast cancer histopathology images. In *Proc. Int. Conf. on Biomedical Engineering and Informatics*, 2008.